

Demystifying Freeze-In Dark Matter at the LHC

Kyu Jung Bae,^{1, 2,*} Myeonghun Park,^{1, 3, †} and Mengchao Zhang^{4, 1, ‡}

¹*Center for Theoretical Physics of the Universe, Institute for Basic Science, Daejeon 34126, Korea*

²*Department of Physics, Kyungpook National University, Daegu 41566, Korea*

³*Institute of Convergence Fundamental Studies and School of Liberal Arts,*

Seoultech, 232 Gongneungro, Nowon-gu, Seoul, 01811, Korea

⁴*Department of Physics and Siyuan Laboratory, Jinan University, Guangzhou 510632, P.R. China*

Freeze-in mechanism provides robust dark matter production in the early universe. Due to its feeble interactions, freeze-in dark matter leaves signals at colliders which are often involved with long-lived particle decays and consequent displaced vertices (DV). In this paper, we develop a method to read off mass spectrum of particles being involved in the DV events at the LHC. We demonstrate that our method neatly works under a limited statistics, detector resolution and smearing effects. The signature of DV at the LHC can come from either highly suppressed phase-space or a feeble coupling of particle decay processes. By measuring invisible particle mass spectrum, one can discriminate these two cases and thus extract information of dominant freeze-in processes in the early universe at the LHC.

I. INTRODUCTION

Particle dark matter (DM) is strongly supported by plethora of cosmological and astrophysical evidences (for reviews on particle dark matter see Ref. [1–3]). Since there is no proper candidate of DM in the standard model (SM), it is considered as one of the most prominent clues to go beyond the SM. The freeze-in mechanism provides a plausible answer to the origin of particle DM in the primeval Universe [4], and also an intriguing set of DM searches in broad area (*e.g.* non-thermal distribution of DM and its impacts [5–10], DM direct detection [11, 12], the large hadron collider (LHC) searches [13–16])¹ although it generically contains tiny interactions with visible particles.

On the contrary to the conventional freeze-out dark matter, the freeze-in dark matter never reaches the equilibration with the thermal plasma. Due to its tiny interaction strength, instead, DM annihilation processes are always inefficient and thus produced DM particles are accumulated as the Universe expands. Hence the correct DM abundance can be achieved despite of feeble interactions [4]. Moreover, the production processes involve renormalizable couplings, so they become more important at low temperature and consequently dominant number of DM particles are produced near the threshold mass scale of the production processes. Below the threshold scale, the production processes are highly suppressed by Boltzmann factor. Therefore, DM abundance is independent of high temperature physics, *i.e.*, reheating after primordial inflation, but is dependent on details of production processes which are *determined by DM particle interactions*.

The feeble nature of DM implies another observable footprints if the DM mass is $\mathcal{O}(1)$ keV. Since DM particles are not equilibrated after being produced, their initial phase space distribution does not change but is simply redshifted during the cosmic expansion. As pointed out in the literature [9, 10], phase space distribution of DM depends on its production channels: 2-body decay, 3-body decay, *s*-channel and *t*-channel scattering, *etc.* Such non-thermal distribution of DM particles impacts on small scale structures and can be probed by the Ly- α forest observation [18–25].

Along with the cosmology, collider study also shows robust signatures of the freeze-in dark matter model. During the freeze-in processes, DM particles come out from thermal plasma of visible particles via feeble interactions between the dark sector and visible sector. It implies the events at colliders where visible particles are produced in pairs and decay into DM particles plus visible particles. For example, higgsino pairs are produced and decay into axinos and higgs bosons. In virtue of its tiny coupling, such decays show a signature of the displaced vertex (DV) at hadron colliders.² The DV searches at the LHC have been considered to investigate various long-lived particles and have increased the sensitivity. In addition, a possible improvement at the high-luminosity (HL) LHC with precision timing information would suppress SM backgrounds leading to a better sensitivity of such long-lived particle searches [27, 28].

In order to examine genuine properties of the freeze-in dark matter model at hadron colliders, we need to go one step further. The DM abundance and distribution are determined by couplings and mass spectrum of the dark sector including the DM component. Thus it is essential to extract the mass information from DV events at colliders. In the case of prompt decay events, kinematic analyses require large number of events to read off

* kyujung.bae@knu.ac.k

† parc.seoultech@seoultech.ac.kr

‡ mczhang@jnu.edu.cn

¹ For more broad aspects of freeze-in dark matter, readers can find reviews in [17].

² We refer readers to Ref. [26] for a recent review on long-lived particle searches at the LHC.

the end-point in the invariant mass distribution [29]. As pointed out in the early study [30], on the other hand, DV renders mass reconstruction possible in an event-by-event basis, so it allows us to extract mass spectrum of dark sector although a handful of events are available. In reality, however, kinematic reconstruction in an event-by-event basis highly depends on detector effects including smearing of final state visible particles.

In this paper, we present a collider method to reconstruct relevant mass spectrum with only conventional track and calorimeter information. To reduce uncertainties in mass measurement originating from detector smearing effects, we develop a simple “filtering” algorithm, which systematically discards the outliers in mass measurement of DV events. For an illustration of our method, we consider pair production of mother particles (F) and their subsequent decays into dark matter particles (χ) and Z bosons, where Z boson decays into a lepton pair for a precise reconstruction.

This paper is organized as follows. In Sec. II, a brief review on freeze-in dark matter is given to argue why the long-lived particle at the LHC is appropriate to examine cosmological freeze-in dark matter scenarios. In Sec. III, we explain kinematic relations in events with DV to reconstruct masses of the decaying particle F and dark matter particle χ . In Sec. IV, we demonstrate how much a simple filtering algorithm enhances accuracy by removing events which have strong smearing effects from a detector. Finally we present our result in mass reconstructions with various benchmark points at the HL-LHC.

II. A BRIEF REVIEW ON FREEZE-IN DARK MATTER

In freeze-in dark matter models, DM particles have tiny *renormalizable* couplings with thermal plasma by which the freeze-in processes are mediated. In the following, we will explain the freeze-in mechanism with a toy example.

Suppose that DM particles are produced by decay of particle A which is in thermal equilibrium, *i.e.* $A \rightarrow B + \chi$. Here we assume B is also in thermal equilibrium. In this case, dark matter production rate is determined by decay width of A , Γ_A . The dominant production occurs when the plasma temperature T is around m_A . For $T < m_A$, population of A is highly suppressed by the Boltzmann factor, so the production process becomes ineffective. One finds the yield of DM particles [4, 31],

$$\begin{aligned} Y_\chi &\approx \frac{135g}{4\pi^4 g_*^{3/2}} \frac{M_P \Gamma_A}{m_A^2} \int_0^\infty z^3 K_1(z) dz \\ &\approx 10^{-3} \frac{M_P \Gamma_A}{m_A^2}, \end{aligned} \quad (2.1)$$

where g is the degrees of freedom of A , g_* is the effective degrees of freedom of thermal plasma M_P is the reduced Planck mass, and $K_1(z)$ is the first modified Bessel function of the second kind. In the second line, we have taken

$g_* = 100$. For the decay of A via renormalizable coupling λ , the decay width is given by

$$\Gamma_A \sim \frac{1}{8\pi} \lambda^2 m_A. \quad (2.2)$$

The yield becomes

$$Y_\chi \sim 4 \times 10^{-5} \lambda^2 \frac{M_P}{m_A}, \quad (2.3)$$

and the DM density is given by

$$\begin{aligned} \Omega_\chi h^2 &\sim 2.8 \times 10^8 Y_\chi \left(\frac{m_\chi}{\text{GeV}} \right) \\ &\sim 0.1 \left(\frac{\lambda}{10^{-8}} \right)^2 \left(\frac{200 \text{ GeV}}{m_A} \right) \left(\frac{m_\chi}{10 \text{ keV}} \right). \end{aligned} \quad (2.4)$$

Therefore, one can see that the freeze-in process provides the correct DM abundance in a wide range of couplings and DM masses although the coupling is tiny. For the coupling $\lambda \sim 10^{-8}$, DM mass is of order keV, so it can be warm dark matter (WDM) and may be probed by small scale observables [5–10]. For even smaller coupling, $\lambda \sim 10^{-12}$, on the other hand, weak scale DM mass (~ 100 GeV) is possible so that DM can be cold dark matter (CDM).

In most of freeze-in DM models, scattering processes are also accompanied by the decay processes. One can find a process like $A + C \rightarrow \chi + D$ (t -channel mediated by B) where C and D are also in thermal equilibrium. The single processes are normally less effective than the decay processes due to the suppression in the kinematic phase factor. In some cases, nonetheless, the scattering process can be enhanced by large number of degrees of freedom of accompanying particles C and D , so it can make sizable contributions to the DM production (see Ref. [32, 33] for axino production cases). In addition, there may exist decay processes with more than 2 final state particles. However, this contribution is more suppressed than 2-body decays by the kinematic phase factor, so is typically subdominant.

In the case where decay and scattering processes are “co-resident,” more interestingly, mass difference between A and B can determine the relative ratio of decay contribution and scattering contribution as well as the phase space distribution. In principle, if $m_A - m_B \ll m_A$, the kinetic energy of produced DM can be arbitrarily small. Under these circumstances, decay process become very inefficient. Nevertheless, the scattering process does not alter dramatically, so it dominates the phase space distribution and relic abundance [10]. Extracting mass spectrum at collider experiments may enable us to infer which process is dominant in freeze-in DM production.

At colliders, direct production of χ is impossible since its coupling to SM particles are too small. However, its mother particle (we named A in the above example) can be produced in the collision experiments. If A is the lightest parity-odd particle in the visible sector (*e.g.*, higgsino in the minimal supersymmetric standard model), it can

decays only to DM particle with decay width in Eq. (2.2). The decay length at the collider is

$$\frac{1}{\Gamma_A} \sim (1.7 \text{ ns or } 50 \text{ cm}) \times \left(\frac{10^{-8}}{\lambda} \right)^2 \left(\frac{200 \text{ GeV}}{m_A} \right). \quad (2.5)$$

For the freeze-in DM with $m_\chi \sim 10 \text{ keV}$ and $\lambda \sim 10^{-8}$, DV length is of order 10 cm, and thus this gives *nearly the best sensitivity* for DV searches at the LHC [34] while it gives dominant dark matter abundance.

For the larger dark matter mass, $m \sim 100 \text{ GeV}$, smaller coupling $\lambda \sim 10^{-12}$ is required to obtain the correct relic abundance in standard cosmology. If this is the case, the decay length is too long to be covered by DV searches. Such region, instead, may be covered by an additional long-lived particle detector outside of the LHC detectors [35]. However, even in the case of large dark matter mass, there are viable non-standard cosmological scenarios leading to the correct relic abundance. If the dark matter mass is around 100 GeV and coupling is of order 10^{-8} , the freeze-in process overproduces DM particles. In such a case, large entropy dilution of factor $10^7 - 10^8$ is necessary to suppress freeze-in processes properly. In a scenario where the DM freeze-in occurs during an early matter dominated era (*i.e.*, $T_R \ll 100 \text{ GeV}$), relatively large coupling $\lambda \sim 10^{-8}$ still provides a viable DM scenario with the correct relic DM abundance [36]. In a scenario in the fast-expanding Universe [37], a similar dilution effect is possible so that viable freeze-in DM model is possible with $m_\chi \sim 100 \text{ GeV}$ and $\lambda \sim 10^{-8}$. In another freeze-in DM model [5, 6], DM particle can be produced by decay of frozen-out particles rather than directly produced from thermal plasma. In such a case, DV searches at the LHC covers the freeze-in DM in indirect way by showing kinematic structure of particle decaying into the DM particle.

In summary, the current and future DV searches for decay length of order 10 cm will be good probes of freeze-in WDM region and part of heavy freeze-in DM models. Once we observe an excess of DV signals above the expected background in the future, analyses on mass spectrum by using the kinematic techniques will be essential to reflect DM production process in the early Universe. In next section, we show kinematic relations to reconstruct mass of mother particle and dark matter particle.

III. KINEMATICS OF DISPLACED VERTEX

We consider a case where the LHC produces pair of unstable particles (F_1, F_2). These particles will decay into dark matter χ and Z boson. As we have not seen any hints of dark matter at the LHC by Run 2, we do not expect to have enough statistics even for a discovery by the end of the HL-LHC. Thus we need to consider a method which provides (m_F, m_χ) in the event-by-event basis, not through the accumulated information. To measure (m_F, m_χ) with a single event, we need to reconstruct

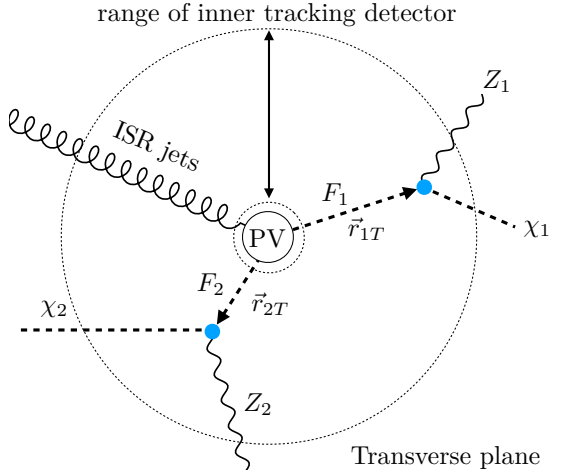


FIG. 1. Positions of two DVs are denoted by \vec{r}_1 and \vec{r}_2 (dashed arrows). Visible (reconstructable) particles are marked with solid lines while invisible particles with dashed ones. Dotted circles represents inner and outer boundary of “inner tracking detector(ID)” with cylindrical radius of $\mathcal{O}(10) - \mathcal{O}(10^3)$ mm. PV stands for primary vertex.

four-momentum of dark matter particles (χ_i). As the number of unknowns from χ_i is eight in total, we need to achieve the same number of constraints using kinematics.

At the LHC detector, F_i will leave a DV, denoted by \vec{r}_i , when it decays into $Z_i (\rightarrow \ell^+ \ell^-)$ and χ_i as in Fig. 1. Due to the charge neutrality F_i , a three momentum vector $\vec{p}_{(F_i)}$ is proportional to \vec{r}_i . This provides two constraints for the direction of each $\vec{p}_{(F_i)}$, resulting in four constraints in total. If we specify a direction of DV in a spherical coordinate (\hat{r}_i : unit vector directing \vec{r}_i),

$$\hat{r}_i = (\sin \theta_i \cos \phi_i, \sin \theta_i \sin \phi_i, \cos \theta_i), \quad (3.1)$$

we can express three momentum $\vec{p}_{(F_i)}$ in terms of DV position vector \hat{r}_i ,

$$\vec{p}_{(F_i)} = |\vec{p}_{(F_i)}| \hat{r}_i. \quad (3.2)$$

In conventional searches for dark matter at the LHC, we utilize a momentum conservation in the transverse plane as we do not see the trace of dark matter directly. With this, we have two constraints:

$$\vec{P}_T = \sum_i \vec{p}_{T(\chi_i)} = - \left(\vec{p}_{T(\text{ISR})} + \sum_i \vec{p}_{T(Z_i)} \right). \quad (3.3)$$

This can be simply translated into a condition for $\vec{p}_{(F_i)}$:

$$\sum_i \vec{p}_{T(F_i)} = -\vec{p}_{T(\text{ISR})}. \quad (3.4)$$

The existence of ISR jets is important to identify dark matter at the LHC. For example, ISR jets are required for the most conventional dark matter searches [38, 39] and for utilizing information from a timing layer [27, 28]. For

the case of $\mathcal{O}(100 - 1000)$ GeV mass scale of F , there are non-negligible number of events with $p_{T(\text{ISR})} \simeq \mathcal{O}(10 - 100)$ GeV [40, 41] and we can utilize this information to extract properties of dark matter at the LHC [42, 43]. In our case, we use $p_{T(\text{ISR})}$ to reconstruct three-momenta $\vec{p}_{T(F_i)}$ by combining Eq. (3.2) and Eq. (3.4),

$$\sum_i (|\vec{p}_{T(F_i)}| \hat{r}_i T) = -\vec{p}_{T(\text{ISR})}. \quad (3.5)$$

If we express above equation more specifically, it can be written as a 2×2 matrix equation,

$$\begin{pmatrix} \sin \theta_1 \cos \phi_1 & \sin \theta_2 \cos \phi_2 \\ \sin \theta_1 \sin \phi_1 & \sin \theta_2 \sin \phi_2 \end{pmatrix} \begin{pmatrix} |\vec{p}_{T(F_1)}| \\ |\vec{p}_{T(F_2)}| \end{pmatrix} = -\begin{pmatrix} |\vec{p}_{T(\text{ISR})}| \cos \phi \\ |\vec{p}_{T(\text{ISR})}| \sin \phi \end{pmatrix}, \quad (3.6)$$

where ϕ is the azimuthal angle of $\vec{p}_{T(\text{ISR})}$ in a transverse plane. This provides a solution for $|\vec{p}_{T(F_i)}|$ in terms of directional angles (ϕ_i, θ_i) of DVs,

$$\begin{aligned} |\vec{p}_{(F_1)}| &= -\frac{|\vec{p}_{T(\text{ISR})}| \sin(\phi - \phi_2)}{\sin \theta_1 \sin(\phi_1 - \phi_2)}, \\ |\vec{p}_{(F_2)}| &= \frac{|\vec{p}_{T(\text{ISR})}| \sin(\phi - \phi_1)}{\sin \theta_2 \sin(\phi_1 - \phi_2)}. \end{aligned} \quad (3.7)$$

When ISR jet becomes soft, Eq. (3.6) turns into an indeterminate system. In the limit of $p_{T(\text{ISR})} \ll \sqrt{\hat{s}}$ where $\sqrt{\hat{s}}$ is the hard scale of an event, the difference $\phi_1 - \phi_2$ can be approximated as

$$\phi_1 - \phi_2 \simeq \pi - \frac{2p_{T(\text{ISR})}}{\sqrt{\hat{s}}} \left(1 - \frac{4m_F^2}{\hat{s}} \right)^{-\frac{1}{2}} \rightarrow \pi. \quad (3.8)$$

As Eq. (3.6) has a factor $\sin(\phi_1 - \phi_2)$ in its determinant, it is required to have non-negligible $p_{T(\text{ISR})}$ to have a numerically stable solution for $|\vec{p}_{(F_i)}|$.

To extract information on masses of invisible particles, we convert solution of momenta into masses using the energy conservation as

$$\sqrt{m_{F_i}^2 + |\vec{p}_{(F_i)}|^2} = E_{Z_i} + \sqrt{m_{\chi_i}^2 + |\vec{p}_{(\chi_i)}|^2}. \quad (3.9)$$

From this, we have a functional dependence of m_{F_i} on m_{χ_i} as

$$m_{F_i} = \sqrt{\left(E_{Z_i} + \sqrt{|\vec{p}_{(\chi_i)}|^2 + m_{\chi_i}^2} \right)^2 - |\vec{p}_{(F_i)}|^2}. \quad (3.10)$$

Here the three-momentum of χ_i is given by $\vec{p}_{(\chi_i)} = |\vec{p}_{(F_i)}| \hat{r}_i - \vec{p}_{(Z_i)}$. So far we use only six constraints to reconstruct a three-momentum of $\vec{p}_{(F_i)}$. We can have two more constraints from our physics motivation where we assume the symmetric condition of $m_{F_1} = m_{F_2}$ and $m_{\chi_1} = m_{\chi_2}$. Thus we have eight constraints enough to measure (m_F, m_χ) even with one event. To illustrate how one can use Eq. (3.10), we take an event with $(m_F, m_\chi) = (200, 50)$ GeV. In Fig. 2, each function for m_{F_i} in Eq. (3.10) is presented either a blue or a orange line with a crossing point as the solution for (m_F, m_χ) .

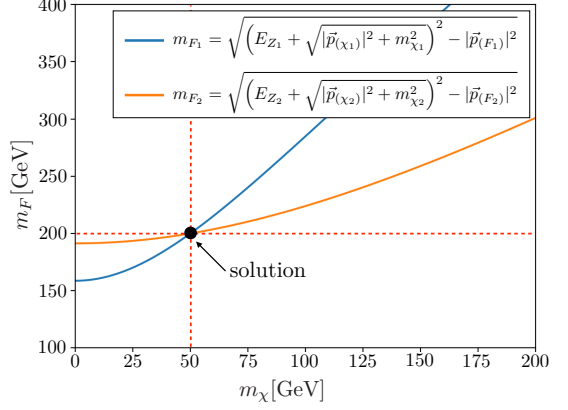


FIG. 2. The functional dependence of m_{F_i} on m_{χ_i} in a specific event is presented as blue and magenta lines according to Eq. (3.10). The event is generated at the parton level with a study point of $(m_F, m_\chi) = (200, 50)$ GeV. For $m_{F_1} = m_{F_2}$ and $m_{\chi_1} = m_{\chi_2}$, the crossing point of two equations gives the solution for m_F and m_χ .

IV. THE HL-LHC STUDY

A. Detector effects with limited number of events

We consider a channel where DVs can be marked by tracing the origin of Z boson production using clean tracks of leptons from $Z \rightarrow \ell^+ \ell^-$ for a precise measurement compared to hadronically decaying Z . However in the LHC detectors, there are uncertainties from (1) measurements of lepton momenta, which can be modeled with 2% uncertainty [44, 45], (2) DV position resolution with a conservative value of 0.5 mm [46], and (3) the missing transverse energy \cancel{E}_T resolution of 10% in the region of $\cancel{E}_T > 200$ GeV [47]. These smearing effects will result in incorrect solutions for Eq. (3.10).

To numerically point this out, we simulate events with the study point of $(m_F, m_\chi) = (250, 50)$ GeV using Monte Carlo simulations by modeling smearing effects with Gaussian functions. As we discussed earlier, $p_{T(\text{ISR})}$ can enhance a numerical stability against smearing effects. We can observe this clearly in Fig. 3 where we divide Monte Carlo events according to the range of $p_{T(\text{ISR})}$. In reality, however, we have $\mathcal{O}(10)$ events after cuts at the HL-LHC, so we cannot rely on the high $p_{T(\text{ISR})}$ configurations as most of events are located at low $p_{T(\text{ISR})}$. Thus we need to develop another method to reduce smearing effects.

To achieve this goal, we develop a simple filtering algorithm. Basically we rely on the fact that events are independent of one another. Thus we focus on the clustering structure of solutions near the true mass point in (m_F, m_χ) solution-space;

- Each solution is treated as a vector \vec{v}_i at $m_F - m_\chi$ plane with $\vec{v}_i = (m_{F_i}, m_{\chi_i})$.

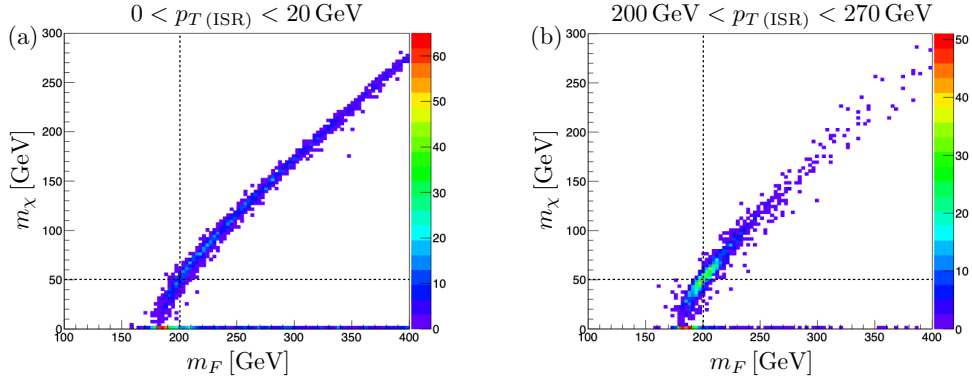


FIG. 3. Distribution of solutions in Eq.(3.10) for a mass spectrum $(m_F, m_\chi) = (250, 50)$ GeV. We use 2000 events for each $p_{T(\text{ISR})}$ region using standard parton-level Monte Carlo simulations with Gaussian smearing for detector effects.

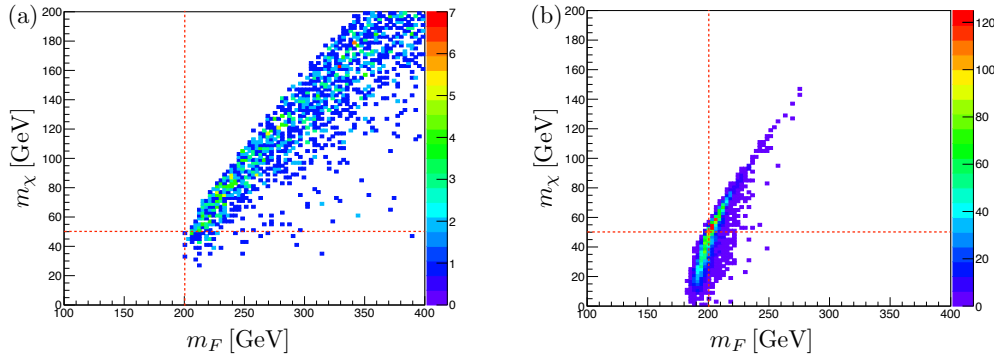


FIG. 4. We show the result of 5000 pseudo-experiments (a) without (b) with the filtering algorithm. We have only 20 events per one pseudo-experiment. For each experiment, we take the mean values for mass measurement. The mass spectrum is the same as in Fig 3.

- For each \vec{v}_i , we measure an ‘‘average distance’’ d_i ,

$$d_i = \frac{1}{N} \sum_{j=1}^N |\vec{v}_i - \vec{v}_j|, \quad (4.1)$$

where N is the total number of solution vectors,

- Remove the \vec{v}_i with largest d_i from our vector list,
- Calculate all d_i again (only use the remaining vectors), and remove the vector with largest average distance. Repeat this process until only half of the vectors remain.

This ‘‘filtering’’ algorithm is neatly dropping bad solutions in a simple and systematic way.

B. Numerical studies with benchmark points

To illustrate our method with realistic situations at the HL-LHC, we consider four benchmark points divided by the scale of m_F and a mass splitting of $\{m_F - (m_\chi + m_Z)\}/m_F$ as in Tab.I. For benchmark

B.P.	m_F [GeV]	m_χ [GeV]	$c\tau$ (mm)	N_{events} @ HL-LHC
A	200	0	100	30
B	200	108	100	20
C	800	0	100	12
D	800	708	100	24

TABLE I. Four benchmark points are illustrated. As the LHC detector is not sensitive to probe a mass scale less than $\mathcal{O}(1)$ GeV, we fix $m_\chi = 0$ for the mass scale of $\mathcal{O}(1-100)$ keV. N_{events} is determined by recasting current LHC searches. These numbers are after baseline selection cuts.

points B and D, the mass splittings are highly suppressed, *i.e.*, $\{m_F - (m_\chi + m_Z)\}/m_F \leq \mathcal{O}(1)\%$ while mass splittings are more than 50% in A and C. Thus if we measure mass spectrum (m_F, m_χ) precisely, we can identify where the lifetime of m_F comes either from suppressed phase-space of small mass splitting or from very small coupling of $F-\chi-Z$. Here we consider the same lifetime of F ($c\tau = 100$ mm) to focus on kinematic differences and performance of our method which relies only on the

reconstruction of $\vec{p}_{(F_i)}$. By recasting current long-lived particle search of ATLAS [34], we expect 30, 20, 12 and 24 events, respectively for benchmark point A, B, C and D at the HL-LHC. We describe detailed information of recasting procedure in Appendix A.

For parton-level Monte Carlo simulations, we use **MadGraph5** [48] to generate events with “MLM” jet matching algorithm [49] implemented in **Pythia8** [50] for ISR jets. To cluster ISR jets, we use **Fastjet** [51] with anti- k_t algorithm [52]. For detector effects, we consider detector geometries and smearing effects as we described above. Finally we choose 14 TeV collision energy and 3 ab^{-1} luminosity for the HL-LHC. As we need to enhance precision for DV, we focus only on leptonic channels of Z decays. For baseline selection cuts, we require

- missing transverse energy $\cancel{E}_T > 200 \text{ GeV}$ to improve the \cancel{E}_T resolution [47],
- 4 electrons or muons with $p_T > 10 \text{ GeV}$ in the final state,
- 2 DVs to be reconstructed inside the inner detector ($4 \text{ mm} < L_{xy} < 1 \text{ m}$ and $|L_z| < 1 \text{ m}$) where DVs are reconstructed by displaced tracks with impact parameter larger than 2 mm and $p_T > 1 \text{ GeV}$, two tracks of each DV to be matched to 2 leptons, and both DV mass m_{DV} to be larger than 80 GeV .³

Due to detector effects and limited statistics, the mass measurement based on track information has large uncertainties. In order to improve the precision, we apply filtering algorithm. It is worth mentioning a subtlety in solving Eq. (3.10) especially when a dark matter is very light. There are cases where two lines in FIG. 2 do not cross due to smearing effects. As $m_{F_i}(m_{\chi_i})$ is an increasing function, we take $m_{\chi} = 0$ and $m_F = (m_{F_1}(m_{\chi_1} = 0) + m_{F_2}(m_{\chi_2} = 0)) / 2$ for a solution.

For benchmark points in Tab. I, we perform 5000 pseudo-experiments to reduce statistical fluctuations. In Table II, we tabulate the most probable mass values for each benchmark point and also estimated statistical errors of pseudo-experiments which are defined by the “root-mean-square (RMS)” value with respect to the most probable values $\text{RMS} = \sqrt{\sum_{i=1}^N (m_i - m^{\text{peak}})^2 / N}$, where m^{peak} is the most probable value and N is the number of pseudo experiments. For benchmark points A, B, and D, the results show good precision, where the errors are around 10% of mother particle mass. For benchmark point C, on the other hand, RMS error is around 30 – 45% of mother particle mass. This mainly comes from small statistics as C has only 12 events after cuts which has factor 1/2 - 1/3 reduction compared to other benchmark points.

³ It is not likely that background processes have $m_{\text{DV}} > 80 \text{ GeV}$ [34], so this cut leads background-free analyses.

B. P.	$(m_F, m_\chi)^{\text{true}}$	RMS
	$(m_F, m_\chi)^{\text{peak}}$	
A	(200, 0)	(7.3, 13)
	(208, 14)	
B	(200, 108)	(14, 15)
	(199, 105)	
C	(800, 0)	(250, 360)
	(835, 0)	
D	(800, 708)	(79, 80)
	(792, 694)	

TABLE II. Peak measured values and root-mean-squares (RMS) for four benchmark points. Numbers are in GeV unit.

In the following, we discuss more direct implication of the above analyses in the freeze-in dark matter scenarios. As argued in Ref. [10], as the phase space of a mother particle decay is highly suppressed, the distribution of DM produced from this decay process becomes colder. Meanwhile, the distribution of DM produced by 2-to-2 scattering processes remains almost the same. This feature can be probed by observations such as Ly- α forest data if the DM mass is of order keV. Therefore, by observing mass spectrum of DM sector at the LHC, we can infer the relative “warmness” of DM distribution. In order to illustrate this situation, we introduce an additional benchmark point E, on which $(m_F, m_\chi) = (100, 0) \text{ GeV}$, $c\tau = 100 \text{ mm}$. The expected number of events after baseline selection cuts at the HL-LHC is 10. At the LHC, we measure $(m_F, m_\chi)^{\text{peak}} = (101, 0) \text{ GeV}$ with statistical deviation $\text{RMS} = (81, 47) \text{ GeV}$ from 5K pseudo experiments. Thus, even though we have uncertainties in determining mass spectrum due to the limited statistics, we will have hints of dark matter temperature of our universe from the HL-LHC.

V. CONCLUSIONS

We develop a pure kinematic method to determine mass spectrum involving DVs at the LHC by locating visible particle track inside inner tracking detector. To measure mass spectrum, we assume conditions $(m_{F_1} = m_{F_2})$ and $(m_{\chi_1} = m_{\chi_2})$ for both decay chains. We also require ISR jets not to have back-to-back configuration between F 's which results in a null solution in reconstructing three momentum vectors of F 's. Large ISR can enhance a numerical stability for the determination of mass spectrum, but we would not have enough statistics to focus on the large $p_{T(\text{ISR})}$ region at the HL-LHC.

In this study, we consider only $\mathcal{O}(10)$ events with detector smearing effects. The performance of the mass measurements gets degraded due to imprecise information on \cancel{E}_T and four vectors of leptons. To achieve satisfactory performance with small number of events, we

propose a simple and systematic method which removes solutions in the mass reconstruction with large errors.

We have demonstrated that one can achieve within $\mathcal{O}(10)\%$ -level precision on mass measurements at the HL-LHC. This result from the HL-LHC enables us to understand the origin of DV signals, either due to a suppressed phase space or due to a feeble coupling of decaying particle. In this respect we can see a relationship between the freeze-in mechanism in the early universe and DV signature at the LHC.

Finally, as we do not rely on any new features of upcoming detector upgrades, our proposed method is orthogonal to other studies with utilizing timing information [27, 28]. One can enhance a precision in mass measurements by combining results from both methods once the LHC identifies DV signals from a new physics.

ACKNOWLEDGMENTS

This work was supported by IBS under the project code IBS-R018-D1. MP is supported by Basic Science Research Program through the National Research Foundation of Korea Research Grant NRF-2018R1C1B6006572. MZ is supported by the National Natural Science Foundation of China (Grant No. 11947118). This work was performed in part at Aspen Center for Physics, which is supported by National Science Foundation grant PHY-1607611.

Appendix A: Recasting of Current long-lived particle searches

We recast the ATLAS long-lived massive particles search report [34] to estimate the upper limit of $\sigma(pp \rightarrow FF)$. There are another long-lived particle searches, for example, searches with displaced jets in the ATLAS [53], which do not have sensitivity for our scenario as they need information of calorimeters.

Here we briefly describe cut-flow used in the ATLAS report [34].

- Transverse missing energy $\cancel{E}_T \geq 250 \text{ GeV}$.
- 75% of events need to have at least one trackless jet with $p_T > 70 \text{ GeV}$ or at least two trackless jets with $p_T > 25 \text{ GeV}$. For other 25% events there is no requirement on trackless jet. Trackless jet is defined to be a jet with $\sum p_T^{\text{track}} < 5 \text{ GeV}$.
- At least one DV needs to be reconstructed in fiducial region of inner detector within a transverse position $4 \text{ mm} < L_{xy} < 300 \text{ mm}$ and longitudinal position $|L_z| < 300 \text{ mm}$. DV is reconstructed by displaced tracks with impact parameter larger than 2 mm and $p_T > 1 \text{ GeV}$. More than five displaced tracks (N_{tracks}) from a DV are required, and reconstructed mass with tracks from DV (m_{DV}) needs to be larger than 10 GeV .
- 42% fiducial volume need to be discarded due to huge backgrounds from hadronic interaction in material rich region.

DV tagging efficiency is a function of its position, N_{tracks} , and m_{DV} . As suggested in [54], we perform our DV tagging by utilizing detailed information provided by ATLAS group in the auxiliary information of [34]. Acceptances of our 4 benchmark points after performing above selection criteria are listed in Tab. III. Acceptances for compressed spectrum B and D are much smaller than large mass splitting spectrum A and C as compressed spectrum does not provide large enough \cancel{E}_T as in Fig. 5.

B.P.	Acceptance	$\sigma(pp \rightarrow FF)_{13 \text{ TeV}}^{\max}$	$\sigma(pp \rightarrow FF)_{14 \text{ TeV}}^{\max}$
A	0.63%	14.43	17.56
B	0.14%	64.41	78.41
C	6.76%	1.35	1.87
D	0.52%	17.62	24.34

TABLE III. Acceptance, upper limits on production cross-section at 13TeV, and recasted cross-section at 14TeV LHC. Values are in fb unit.

-
- [1] G. Jungman, M. Kamionkowski, and K. Griest, “Supersymmetric dark matter,” *Phys. Rept.* **267** (1996) 195–373, [arXiv:hep-ph/9506380 \[hep-ph\]](https://arxiv.org/abs/hep-ph/9506380).
- [2] G. Bertone, D. Hooper, and J. Silk, “Particle dark matter: Evidence, candidates and constraints,” *Phys. Rept.* **405** (2005) 279–390, [arXiv:hep-ph/0404175 \[hep-ph\]](https://arxiv.org/abs/hep-ph/0404175).
- [3] G. Bertone and D. Hooper, “History of dark matter,” *Rev. Mod. Phys.* **90** no. 4, (2018) 045002, [arXiv:1605.04909 \[astro-ph.CO\]](https://arxiv.org/abs/1605.04909).
- [4] L. J. Hall, K. Jedamzik, J. March-Russell, and S. M. West, “Freeze-In Production of FIMP Dark Matter,” *JHEP* **03** (2010) 080, [arXiv:0911.1120 \[hep-ph\]](https://arxiv.org/abs/0911.1120).
- [5] A. Merle and M. Totzauer, “keV Sterile Neutrino Dark Matter from Singlet Scalar Decays: Basic Concepts and Subtle Features,” *JCAP* **1506** (2015) 011, [arXiv:1502.01011 \[hep-ph\]](https://arxiv.org/abs/1502.01011).
- [6] J. König, A. Merle, and M. Totzauer, “keV Sterile Neutrino Dark Matter from Singlet Scalar Decays: The Most General Case,” *JCAP* **1611** no. 11, (2016) 038, [arXiv:1609.01289 \[hep-ph\]](https://arxiv.org/abs/1609.01289).
- [7] S. B. Roland and B. Shakya, “Cosmological Imprints of Frozen-In Light Sterile Neutrinos,” *JCAP* **1705** no. 05, (2017) 027, [arXiv:1609.06739 \[hep-ph\]](https://arxiv.org/abs/1609.06739).
- [8] J. Heeck and D. Teresi, “Cold keV dark matter from decays and scatterings,” *Phys. Rev.* **D96** no. 3, (2017)

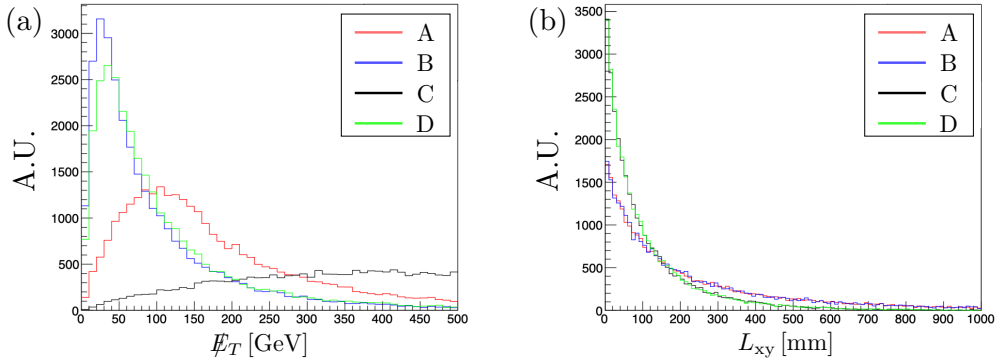


FIG. 5. Distributions of \not{E}_T and L_{xy} for benchmark points. Benchmark points B and D with small mass splittings have lower \not{E}_T distributions than those of A and C. For L_{xy} , C and D with larger m_F have smaller values than the case of A and B. N_{tracks} and m_{DV} distributions are not significantly different among benchmark points.

- 035018, [arXiv:1706.09909 \[hep-ph\]](#).
- [9] K. J. Bae, A. Kamada, S. P. Liew, and K. Yanagi, “Colder Freeze-in Axinos Decaying into Photons,” *Phys. Rev.* **D97** no. 5, (2018) 055019, [arXiv:1707.02077 \[hep-ph\]](#).
 - [10] K. J. Bae, A. Kamada, S. P. Liew, and K. Yanagi, “Light axinos from freeze-in: production processes, phase space distributions, and Ly- α forest constraints,” *JCAP* **1801** no. 01, (2018) 054, [arXiv:1707.06418 \[hep-ph\]](#).
 - [11] R. Essig, J. Mardon, and T. Volansky, “Direct Detection of Sub-GeV Dark Matter,” *Phys. Rev.* **D85** (2012) 076007, [arXiv:1108.5383 \[hep-ph\]](#).
 - [12] T. Hambye, M. H. G. Tytgat, J. Vandecasteele, and L. Vanderheyden, “Dark matter direct detection is testing freeze-in,” *Phys. Rev.* **D98** no. 7, (2018) 075017, [arXiv:1807.05022 \[hep-ph\]](#).
 - [13] G. Barenboim, E. J. Chun, S. Jung, and W. I. Park, “Implications of an axino LSP for naturalness,” *Phys. Rev.* **D90** no. 3, (2014) 035020, [arXiv:1407.1218 \[hep-ph\]](#).
 - [14] A. G. Hessler, A. Ibarra, E. Molinaro, and S. Vogl, “Probing the scotogenic FIMP at the LHC,” *JHEP* **01** (2017) 100, [arXiv:1611.09540 \[hep-ph\]](#).
 - [15] L. Calibbi, L. Lopez-Honorez, S. Lowette, and A. Mariotti, “Singlet-Doublet Dark Matter Freeze-in: LHC displaced signatures versus cosmology,” *JHEP* **09** (2018) 037, [arXiv:1805.04423 \[hep-ph\]](#).
 - [16] G. Bélanger *et al.*, “LHC-friendly minimal freeze-in models,” *JHEP* **02** (2019) 186, [arXiv:1811.05478 \[hep-ph\]](#).
 - [17] N. Bernal, M. Heikinheimo, T. Tenkanen, K. Tuominen, and V. Vaskonen, “The Dawn of FIMP Dark Matter: A Review of Models and Constraints,” *Int. J. Mod. Phys. A* **32** no. 27, (2017) 1730023, [arXiv:1706.07442 \[hep-ph\]](#).
 - [18] M. Viel, J. Lesgourges, M. G. Haehnelt, S. Matarrese, and A. Riotto, “Constraining warm dark matter candidates including sterile neutrinos and light gravitinos with WMAP and the Lyman-alpha forest,” *Phys. Rev.* **D71** (2005) 063534, [arXiv:astro-ph/0501562 \[astro-ph\]](#).
 - [19] U. Seljak, A. Makarov, P. McDonald, and H. Trac, “Can sterile neutrinos be the dark matter?,” *Phys. Rev. Lett.* **97** (2006) 191303, [arXiv:astro-ph/0602430 \[astro-ph\]](#).
 - [20] M. Viel, J. Lesgourges, M. G. Haehnelt, S. Matarrese, and A. Riotto, “Can sterile neutrinos be ruled out as warm dark matter candidates?,” *Phys. Rev. Lett.* **97** (2006) 071301, [arXiv:astro-ph/0605706 \[astro-ph\]](#).
 - [21] M. Viel, G. D. Becker, J. S. Bolton, M. G. Haehnelt, M. Rauch, and W. L. W. Sargent, “How cold is cold dark matter? Small scales constraints from the flux power spectrum of the high-redshift Lyman-alpha forest,” *Phys. Rev. Lett.* **100** (2008) 041304, [arXiv:0709.0131 \[astro-ph\]](#).
 - [22] M. Viel, G. D. Becker, J. S. Bolton, and M. G. Haehnelt, “Warm dark matter as a solution to the small scale crisis: New constraints from high redshift Lyman- α forest data,” *Phys. Rev.* **D88** (2013) 043502, [arXiv:1306.2314 \[astro-ph.CO\]](#).
 - [23] J. Baur, N. Palanque-Delabrouille, C. Yèche, C. Magneville, and M. Viel, “Lyman-alpha Forests cool Warm Dark Matter,” *JCAP* **1608** no. 08, (2016) 012, [arXiv:1512.01981 \[astro-ph.CO\]](#).
 - [24] V. Iršič *et al.*, “New Constraints on the free-streaming of warm dark matter from intermediate and small scale Lyman- α forest data,” *Phys. Rev.* **D96** no. 2, (2017) 023522, [arXiv:1702.01764 \[astro-ph.CO\]](#).
 - [25] C. Yèche, N. Palanque-Delabrouille, J. Baur, and H. du Mas des Bourboux, “Constraints on neutrino masses from Lyman-alpha forest power spectrum with BOSS and XQ-100,” *JCAP* **1706** no. 06, (2017) 047, [arXiv:1702.03314 \[astro-ph.CO\]](#).
 - [26] J. Alimena *et al.*, “Searching for long-lived particles beyond the Standard Model at the Large Hadron Collider,” [arXiv:1903.04497 \[hep-ex\]](#).
 - [27] J. Liu, Z. Liu, and L.-T. Wang, “Enhancing Long-Lived Particles Searches at the LHC with Precision Timing Information,” *Phys. Rev. Lett.* **122** no. 13, (2019) 131801, [arXiv:1805.05957 \[hep-ph\]](#).
 - [28] Z. Flowers, D. W. Kang, Q. Meier, S. C. Park, and C. Rogan, “Timing information at HL-LHC: Complete determination of masses of Dark Matter and Long lived particle,” [arXiv:1903.05825 \[hep-ph\]](#).
 - [29] I. Hinchliffe, F. E. Paige, M. D. Shapiro, J. Soderqvist, and W. Yao, “Precision SUSY measurements at CERN LHC,” *Phys. Rev.* **D55** (1997) 5520–5540,

- [arXiv:hep-ph/9610544 \[hep-ph\]](https://arxiv.org/abs/hep-ph/9610544).
- [30] M. Park and Y. Zhao, “Recovering Particle Masses from Missing Energy Signatures with Displaced Tracks,” [arXiv:1110.1403 \[hep-ph\]](https://arxiv.org/abs/1110.1403).
- [31] E. J. Chun, “Dark matter in the Kim-Nilles mechanism,” *Phys. Rev.* **D84** (2011) 043509, [arXiv:1104.2219 \[hep-ph\]](https://arxiv.org/abs/1104.2219).
- [32] K. J. Bae, K. Choi, and S. H. Im, “Effective Interactions of Axion Supermultiplet and Thermal Production of Axino Dark Matter,” *JHEP* **08** (2011) 065, [arXiv:1106.2452 \[hep-ph\]](https://arxiv.org/abs/1106.2452).
- [33] K. J. Bae, E. J. Chun, and S. H. Im, “Cosmology of the DFSZ axino,” *JCAP* **1203** (2012) 013, [arXiv:1111.5962 \[hep-ph\]](https://arxiv.org/abs/1111.5962).
- [34] **ATLAS** Collaboration, M. Aaboud *et al.*, “Search for long-lived, massive particles in events with displaced vertices and missing transverse momentum in $\sqrt{s} = 13$ TeV pp collisions with the ATLAS detector,” *Phys. Rev.* **D97** no. 5, (2018) 052012, [arXiv:1710.04901 \[hep-ex\]](https://arxiv.org/abs/1710.04901).
- [35] D. Curtin *et al.*, “Long-Lived Particles at the Energy Frontier: The MATHUSLA Physics Case,” [arXiv:1806.07396 \[hep-ph\]](https://arxiv.org/abs/1806.07396).
- [36] R. T. Co, F. D’Eramo, L. J. Hall, and D. Pappadopulo, “Freeze-In Dark Matter with Displaced Signatures at Colliders,” *JCAP* **1512** no. 12, (2015) 024, [arXiv:1506.07532 \[hep-ph\]](https://arxiv.org/abs/1506.07532).
- [37] F. D’Eramo, N. Fernandez, and S. Profumo, “Dark Matter Freeze-in Production in Fast-Expanding Universes,” *JCAP* **1802** no. 02, (2018) 046, [arXiv:1712.07453 \[hep-ph\]](https://arxiv.org/abs/1712.07453).
- [38] **ATLAS** Collaboration, M. Aaboud *et al.*, “Search for new phenomena in final states with an energetic jet and large missing transverse momentum in pp collisions at $\sqrt{s} = 13$ TeV using the ATLAS detector,” *Phys. Rev.* **D94** no. 3, (2016) 032005, [arXiv:1604.07773 \[hep-ex\]](https://arxiv.org/abs/1604.07773).
- [39] CMS Collaboration, C. Collaboration, “Search for new physics in final states with an energetic jet or a hadronically decaying W or Z boson using 35.9 fb^{-1} of data at $\sqrt{s} = 13$ TeV,”.
- [40] J. Alwall *et al.*, “Comparative study of various algorithms for the merging of parton showers and matrix elements in hadronic collisions,” *Eur. Phys. J.* **C53** (2008) 473–500, [arXiv:0706.2569 \[hep-ph\]](https://arxiv.org/abs/0706.2569).
- [41] J. Alwall, K. Hiramatsu, M. M. Nojiri, and Y. Shimizu, “Novel reconstruction technique for New Physics processes with initial state radiation,” *Phys. Rev. Lett.* **103** (2009) 151802, [arXiv:0905.1201 \[hep-ph\]](https://arxiv.org/abs/0905.1201).
- [42] J. L. Feng, S. Su, and F. Takayama, “Lower limit on dark matter production at the large hadron collider,” *Phys. Rev. Lett.* **96** (2006) 151802, [arXiv:hep-ph/0503117 \[hep-ph\]](https://arxiv.org/abs/hep-ph/0503117).
- [43] K. J. Bae, T. H. Jung, and M. Park, “Spectral Decomposition of Missing Transverse Energy at Hadron Colliders,” *Phys. Rev. Lett.* **119** no. 26, (2017) 261801, [arXiv:1706.04512 \[hep-ph\]](https://arxiv.org/abs/1706.04512).
- [44] **ATLAS** Collaboration, G. Aad *et al.*, “Muon reconstruction performance of the ATLAS detector in proton–proton collision data at $\sqrt{s} = 13$ TeV,” *Eur. Phys. J.* **C76** no. 5, (2016) 292, [arXiv:1603.05598 \[hep-ex\]](https://arxiv.org/abs/1603.05598).
- [45] **ATLAS** Collaboration, M. Aaboud *et al.*, “Electron and photon energy calibration with the ATLAS detector using 2015–2016 LHC proton-proton collision data,” *JINST* **14** no. 03, (2019) P03017, [arXiv:1812.03848 \[hep-ex\]](https://arxiv.org/abs/1812.03848).
- [46] **ATLAS** Collaboration Collaboration, “Performance of vertex reconstruction algorithms for detection of new long-lived particle decays within the ATLAS inner detector,” Tech. Rep. ATL-PHYS-PUB-2019-013, CERN, Geneva, Mar, 2019. <https://cds.cern.ch/record/2669425>.
- [47] **ATLAS** Collaboration, M. Aaboud *et al.*, “Performance of missing transverse momentum reconstruction with the ATLAS detector using proton-proton collisions at $\sqrt{s} = 13$ TeV,” *Eur. Phys. J.* **C78** no. 11, (2018) 903, [arXiv:1802.08168 \[hep-ex\]](https://arxiv.org/abs/1802.08168).
- [48] J. Alwall, R. Frederix, S. Frixione, V. Hirschi, F. Maltoni, O. Mattelaer, H. S. Shao, T. Stelzer, P. Torrielli, and M. Zaro, “The automated computation of tree-level and next-to-leading order differential cross sections, and their matching to parton shower simulations,” *JHEP* **07** (2014) 079, [arXiv:1405.0301 \[hep-ph\]](https://arxiv.org/abs/1405.0301).
- [49] M. L. Mangano, M. Moretti, F. Piccinini, and M. Treccani, “Matching matrix elements and shower evolution for top-quark production in hadronic collisions,” *JHEP* **01** (2007) 013, [arXiv:hep-ph/0611129 \[hep-ph\]](https://arxiv.org/abs/hep-ph/0611129).
- [50] T. Sjostrand, S. Mrenna, and P. Z. Skands, “A Brief Introduction to PYTHIA 8.1,” *Comput. Phys. Commun.* **178** (2008) 852–867, [arXiv:0710.3820 \[hep-ph\]](https://arxiv.org/abs/0710.3820).
- [51] M. Cacciari, G. P. Salam, and G. Soyez, “FastJet User Manual,” *Eur. Phys. J.* **C72** (2012) 1896, [arXiv:1111.6097 \[hep-ph\]](https://arxiv.org/abs/1111.6097).
- [52] M. Cacciari, G. P. Salam, and G. Soyez, “The anti- k_t jet clustering algorithm,” *JHEP* **04** (2008) 063, [arXiv:0802.1189 \[hep-ph\]](https://arxiv.org/abs/0802.1189).
- [53] **ATLAS** Collaboration, M. Aaboud *et al.*, “Search for long-lived neutral particles in pp collisions at $\sqrt{s} = 13$ TeV that decay into displaced hadronic jets in the ATLAS calorimeter,” *Eur. Phys. J.* **C79** no. 6, (2019) 481, [arXiv:1902.03094 \[hep-ex\]](https://arxiv.org/abs/1902.03094).
- [54] G. Brooijmans *et al.*, “Les Houches 2017: Physics at TeV Colliders New Physics Working Group Report,” in *Les Houches 2017: Physics at TeV Colliders New Physics Working Group Report*. 2018. [arXiv:1803.10379 \[hep-ph\]](https://arxiv.org/abs/1803.10379). <http://lss.fnal.gov/archive/2017/conf/fermilab-conf-17-664-ppd.pdf>.